

Article

Seasonal Drought Dynamics and the Time-Lag Effect in the MU Us Sandy Land (China) Under the Lens of Climate Change

Fuqiang Wang¹, Ruiping Li^{1,*}, Sinan Wang², Huan Wang¹, Yanru Shi³, Yin Zhang^{1,4}, Jianwei Zhao¹ and Jinming Yang⁵

- ¹ College of Water Conservancy and Civil Engineering, Inner Mongolia Agricultural University, Hohhot 010018, China; wfq19980606@emails.imau.edu.cn (F.W.); zhangyin1987@emails.imau.edu.cn (Y.Z.)
² Yinshanbeilu National Field Research Station of Desert Steppe Eco-Hydrological System, China Institute of Water Resources and Hydropower Research, Beijing 100038, China
³ Taipusi Banner Meteorological Bureau, Taipusi Banner 027000, China
⁴ Department of Water Conservancy and Civil Engineering, Hetao College, Bayannur 015000, China
⁵ State Key Laboratory of Desert and Oasis Ecology, Key Laboratory of Ecological Safety and Sustainable Development in Arid Lands, Xinjiang Institute of Ecology and Geography, Chinese Academy of Sciences, Urumqi 830011, China; yjm@ms.xjb.ac.cn
* Correspondence: nmglrp@imau.edu.cn

Abstract: Sand prevention and control are the main tasks of desertification control. The MU Us Sandy Land (MUSL), one of China's four main deserts, frequently experiences droughts and has a very fragile biological environment. Climate change is the main factor leading to drought, and it may result in more serious drought situations in the future. The Temperature Vegetation Dryness Index (TVDI) was established using land surface temperature and normalized difference vegetation index data. In this paper, we investigate spatial and temporal change characteristics, future change trends, and the time-lag effect of TVDI on climate factors at different scales in MUSL from 2001 to 2020 using Sen + Mann–Kendall trend analysis, Hurstexponent, partial correlation analysis, and lag analysis methods. The results show that (1) the overall drought shows a spatial characteristic of gradually alleviating from west to east (TVDI = 0.6). A significant drying trend dominated 38.5% of the pixels in the fall ($Z = 1.99$), and a highly significant drying trend dominated the rest of the three seasons (Z average = 2.95) and the whole year ($Z = 3.47$). (2) In the future, dry autumn, winter, and the whole year will be dominated by continuous drying, and spring and summer will mainly change from dry to wet. The main relationships between winter TVDI and temperature (-0.06) and precipitation (-0.07) were negative, while evapotranspiration (0.18) showed a positive correlation. The six land use types in spring, summer, fall, and the whole year were primarily non-significantly positively correlated with temperature and evapotranspiration. (3) At the seasonal scale, the sensitive factors in spring and autumn were opposite, with spring TVDI responding quickly to precipitation (0.3 months) and being less sensitive to temperature (1.8 months) and evapotranspiration (2 months). At the interannual scale, desert land TVDI was most sensitive to precipitation (2.6 months) and least responsive to temperature (3 months).

Keywords: TVDI; climate factors; spatial and temporal characteristics; time-lag effect; seasonal drought; MU Us Sandy Land



Citation: Wang, F.; Li, R.; Wang, S.; Wang, H.; Shi, Y.; Zhang, Y.; Zhao, J.; Yang, J. Seasonal Drought Dynamics and the Time-Lag Effect in the MU Us Sandy Land (China) Under the Lens of Climate Change. *Land* **2024**, *13*, 307. <https://doi.org/10.3390/land13030307>

Academic Editor: Luca Salvati

Received: 24 January 2024

Revised: 21 February 2024

Accepted: 26 February 2024

Published: 29 February 2024



Copyright: © 2024 by the authors. Licensee MDPI, Basel, Switzerland. This article is an open access article distributed under the terms and conditions of the Creative Commons Attribution (CC BY) license (<https://creativecommons.org/licenses/by/4.0/>).

1. Introduction

Among the most frequent natural catastrophes worldwide is drought, which is distinguished by its high frequency, protracted time span, and wide effect scope [1]. The environmentally delicate dry and semi-arid regions are particularly vulnerable to the effects of changing climate, and the deterioration of drought poses a huge challenge to the management and protection of ecosystems in these areas [2]. In the northern Chinese agro-pastoral

ecotone, large-scale climate change is characterized by reduced rainfall and increased temperatures, leading to land degradation and agricultural disasters [3]; in addition, human activities change the surface circumstances (such as shifting land utilization, water conservancy project regulation and storage) through direct and indirect ways, and then affect the natural processes, such as hydrological cycle processes, and ultimately act on regional drought [4]. Owing to the combined consequences of intense human behavior and changing climate, drought events occur frequently and persist globally, resulting in serious damage to ecosystem services, depletion of surface and groundwater resources, land desertification, and crop yield reduction, which hinders social and economic sustainable development [5]. Research indicates that the worldwide economic damages resulting from drought were assessed to have reached USD 124 billion between 1998 and 2017. The frequency and length of droughts have grown by 29% since 2000, impacting around 1.4 billion individuals [6]. The temperate dry and semi-arid zones are home to the MUSL, one of the most important ecologically sensitive areas and important agricultural production bases in China. Due to the dual constraints of climate change and overgrazing, rainfall in the region is reduced, aggravating desertification and worsening the drought situation [7,8]. Drought directly causes crop yield reduction in the region and indirectly causes land desertification, further increasing the frequency of extreme climate events such as sandstorms, affecting air quality both inside and outside the region, and adversely affecting the growth of local agriculture and animal husbandry [9,10]. In addition, MUSL is an important part of the ecosystem of the Loess Plateau, which is crucial for windbreak along with sand fixation and maintaining regional ecological balance [11]. Therefore, it is essential to investigate the mechanism as well as pattern underlying drought development in MUSL.

At present, remote sensing has become the main means of drought monitoring, and the drought index is the quantitative expression of drought degree. Numerous researchers have conducted extensive study work with different drought indexes. For example, Zhou et al. [12] used the ESTARFM model to extract vegetation temperature condition index (VTCI) from Sentinel-2 as well as low spatial resolution MODIS images. They then analyzed its relationship with the fused VTCI, applying Terra MODIS VTCI metadata. Their findings demonstrate that the fused VTCI drought monitoring ability is better than Terra MODIS VTCI. However, VTCI is susceptible to cloud cover, vegetation type, sensors, and other factors, resulting in reduced reliability. In 1981, Jackson et al. [13] introduced the crop water stress index (CWSI), which needs to be estimated based on actual transpiration. Due to the complexity and limitations of the estimation method of actual transpiration (the Penman–Monteith formula remains only useful in humid conditions), Liu et al. [14] created a non-parametric method (NP) based on imagery from Landsat 8 and CLDAS materials to calculate realistic evapotranspiration. The Penman–Monteith (P-M) method was used to compute potential evapotranspiration, and the results indicate that CWSI-NM has a stronger relationship with measured soil moisture levels than standard CWSI, making it a dependable method in persistent drought assessment. However, this method depends on specific meteorological conditions. The climatic characteristics of MUSL are low precipitation, high evaporation, and strong wind speed. These extreme and complex environmental conditions affect the accuracy and applicability of CWSI. Tang et al. [15], based on the perpendicular drought index (PDI) and the modified perpendicular drought index (MPDI), assessed the soil humid conditions throughout the crop growing season. Results demonstrate that PDI and MPDI have high applicability in the inversion of soil moisture, but when the vegetation coverage is very high, especially close to 1, it is easy to produce negative values. Wei et al. [16] established a comprehensive drought index (CDI) using spatial principal component analysis (SPCA) and verified it by standardized precipitation evapotranspiration index (SPEI), gross primary productivity (GPP), vegetation condition index (VCI), and soil moisture (SM). The results show that CDI is a reliable drought index in short-term drought monitoring. However, building CDI in northern desert regions and areas with low vegetation cover is challenging due to the lack of ET and PET information.

In summary, the applicability of different drought indices is affected by various factors. Therefore, the selection of drought indices in this study area needs to consider many aspects, including climatic conditions, vegetation coverage, and data coverage. Because VSWI and MPDI are suitable for high vegetation coverage areas, CWSI is suitable for regions with partial vegetation coverage, and PDI is appropriate for monitoring drought in areas with low vegetation coverage or bare surfaces. VTCI is limited to drought research at specific time scales [17,18]. Sandholt et al. [19] mentioned a temperature vegetation drought index (TVDI) using a simplified NDVI-LST feature space. This index combines information from visible, near-infrared, and thermal infrared bands to observe soil moisture. It is particularly suitable for monitoring arid areas with variable climates and significant changes in vegetation cover. The land cover of the MUSL ranges from bare land to areas with partial vegetation coverage and extends to regions with high vegetation coverage in the southern cultivated lands. This distribution aligns well with the vegetation distribution characteristics observed in the LST-NDVI feature space. Many researchers have used TVDI for drought monitoring and compared the monitoring capabilities of other drought indices and achieved good results. For example, Guo et al. [20] employed TVDI to track the features of the drought in Shandong Province between 2011 and 2020. They realized that the east-central region of the province had a severe drought and that TVDI and GLDAS 0–10 cm had a strong correlation. They also found that TVDI had a certain lag on precipitation. Luo et al. [21] constructed TVDI, the vegetation supply water index (VSWI), VCI, and TCI based on MODIS data. Through correlation analysis using observed soil moisture within the 0–20 cm depth range, they found that TVDI exhibited a stronger correlation than the other three remote-sensing drought indices.

In addition, when discussing the influencing factors of drought, particularly in the context of MUSL, the focus has been primarily on temperature, precipitation, topography, and population density [22,23]. However, this approach overlooks crucial climate characteristics associated with MUSL, such as heavy evapotranspiration. By solely analyzing the correlation between drought and climatic factors, there is a risk of underestimating the impact of climate change on drought occurrence. Considering the aforementioned shortcomings, this study considers temperature, precipitation, and evapotranspiration as driving factors. It utilizes lag analysis to quantify the lag period of TVDI in relation to climate factors, aiming to address the underestimation of the influence of climate change on drought occurrence.

Therefore, the objectives for this research were to (1) quantify the extent of drought with autocorrelation of TVDI series data and the effect of climatic factors (including evapotranspiration) on drought in MUSL; (2) analyze the features of the seasonal and annual drought's temporal and spatial spread, the TVDI's variations trends between 20a and the future for various kinds of land use, and the relationship between seasonal drought and seasonal climatic parameters; and (3) explore the reasons for the greatest drought in the spring, the predominance of dry to wet summers and the predominance of persistent drying the whole year in the future, as well as the mechanisms by which TVDI is influenced by climatic factors for multiple types of land use. These objectives aim to provide academic support and a foundation for decision-making regarding the development of agriculture, animal husbandry, and drought early warning systems in MUSL.

2. Study Area and Methods

2.1. Study Area

The MUSL ($36^{\circ}49' \sim 40^{\circ}11' \text{ N}$, $106^{\circ}20' \sim 111^{\circ}00' \text{ E}$) (Figure 1) is a typical semi-arid early agricultural and pastoral area in northern China. The area is seriously decertified and ecologically fragile, situated amid the Ordos Plateau and the Loess Plateau at an elevation of 1000–1600 m. This is mostly made up of grassland and desert in the northwest and cropland and grassland in the southeast (Figure 2a). Situated on the periphery of the East Asian summer monsoon, MUSL experiences a predominantly dry and semi-arid continental climate. The mean temperature has risen from 5.9° C in the northeast to 10.9° C

in the southwest during the previous 20 years (Figure 1f), with low temperatures and dry conditions in the winter and high temperatures and rain in the summer. And the average yearly precipitation is 275.5 mm (Figure 1e), diminishing from southeast to northwest, with the most precipitation throughout the summer and early autumn, and the year seems to be dry. The yearly evapotranspiration average is 94 mm (Figure 1g). Soil moisture content drops by enormous scale afforestation as some of the MUSL's soil moisture is lost via transpiration and returns to the sky [24].

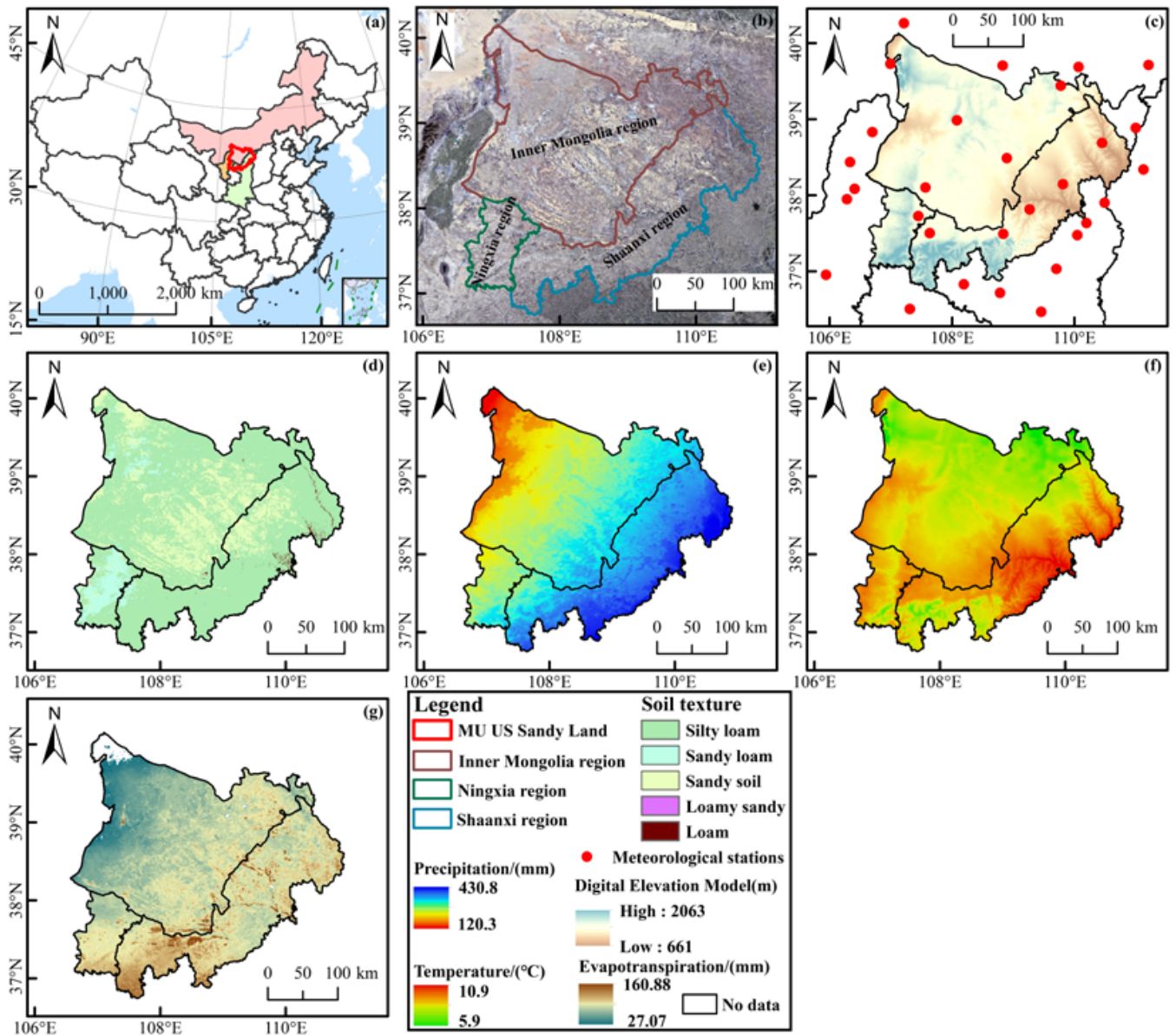


Figure 1. Overview of the research area. (a) Geographic coordinates of MUSL; (b) Inner Mongolia region, Shaanxi region, Ningxia region of MUSL; (c) digital elevation mode and meteorological station; (d) soil texture; (e) precipitation; (f) temperature; (g) ET.

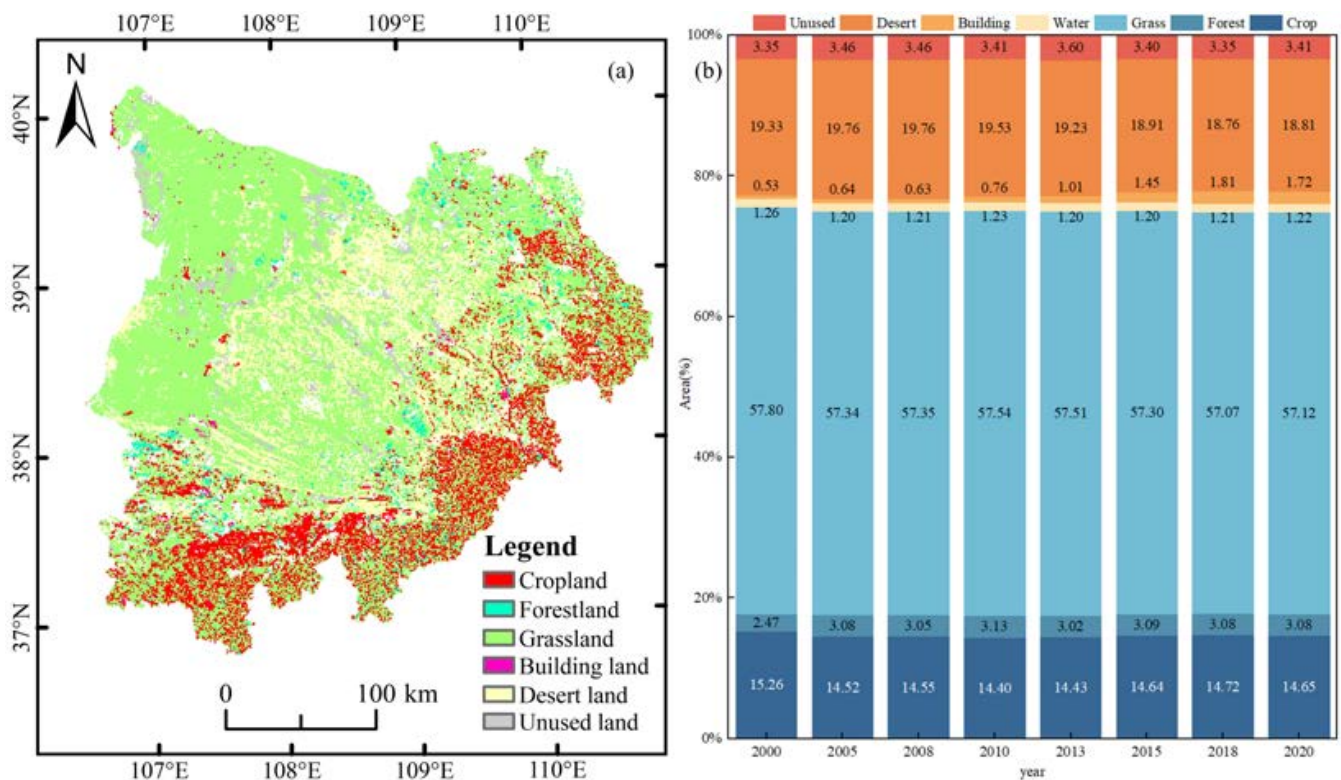


Figure 2. (a) Land use types that have not changed from 2000 to 2020. (b) The percentage of different land utilization categories in various years.

2.2. Data Sources

Land surface temperature (LST) data and the NDVI data, provided by NASA as part of the Modis data products, were taken from the 16d synthesized version of the MOD13A3 product and the 8d synthesized version of the MOD11A2 product, respectively. Pre-processing operations, including format conversion, splicing, projection, cropping, etc., were performed on the HDF-type data through the MODIS Reprojection Tool (MRT). The maximum value synthesis technique was employed to synthesize NDVI and LST data into monthly values. Finally, the LST is corrected, and the correction formula is shown in reference [25]. Evapotranspiration data (ET) were derived from the MOD16A2 product on the NASA website.

Monthly data provided by the China Meteorological Data Center (<http://www.resdc.cn/User> (accessed on 29 August 2023)) for the period 2001–2020 is the basis for the temperature and precipitation data, and meteorological data for 30 stations in the research region were acquired (Figure 1c). Using professional meteorological interpolation software ANUSPLIN (ANUSPLIN VERSION 4.4, The Australian National University Fenner School of Environment and Society, Canberra, Australia) for spatial interpolation, heat and precipitation data were interpolated from point scale to 1 km resolution raster data using a 90 m STRM DEM (digital elevation model) as a covariate. The seasons were classified as follows: winter (January, February, and December of this year), spring (March to May), summer (June to August), and autumn (September to November).

The soil texture data are derived from the National Soil Survey and Soil Series of China data. It employs adaptive depth function fitting, ensemble machine learning, and other methods to generate 250 m resolution raster data for soil sand, clay, and silt content in the 0–30 cm layer. Textural categorization consists of five categories based on USDA classification guidelines: sandy soil, loamy sandy, sandy loam, silty loam, and loam (Figure 1d). Land use data with a 1 km resolution were obtained from the Resource and Environmental Science and Data Centre (<http://www.resdc.cn/> (accessed on 15 July 2023)). The Intersect

tool was used to identify regions where land use types remained relatively unchanged between 2000 and 2020 (Figure 2a), excluding water bodies. The data were reclassified into seven categories: cropland, forestland, grassland, water bodies, built-up land, desert land, and unused land, accounting for 14.61%, 2.37%, 58.71%, 0.56%, 19.25%, and 3.31%, respectively (Figure 2b).

2.3. Methods

Utilizing meteorological and remote sensing data in conjunction with techniques like Sen + MK trend analysis and lag analysis, we examine the spatiotemporal change features and response mechanism of TVDI driving factors. Figure 3 displays the technical flowchart.

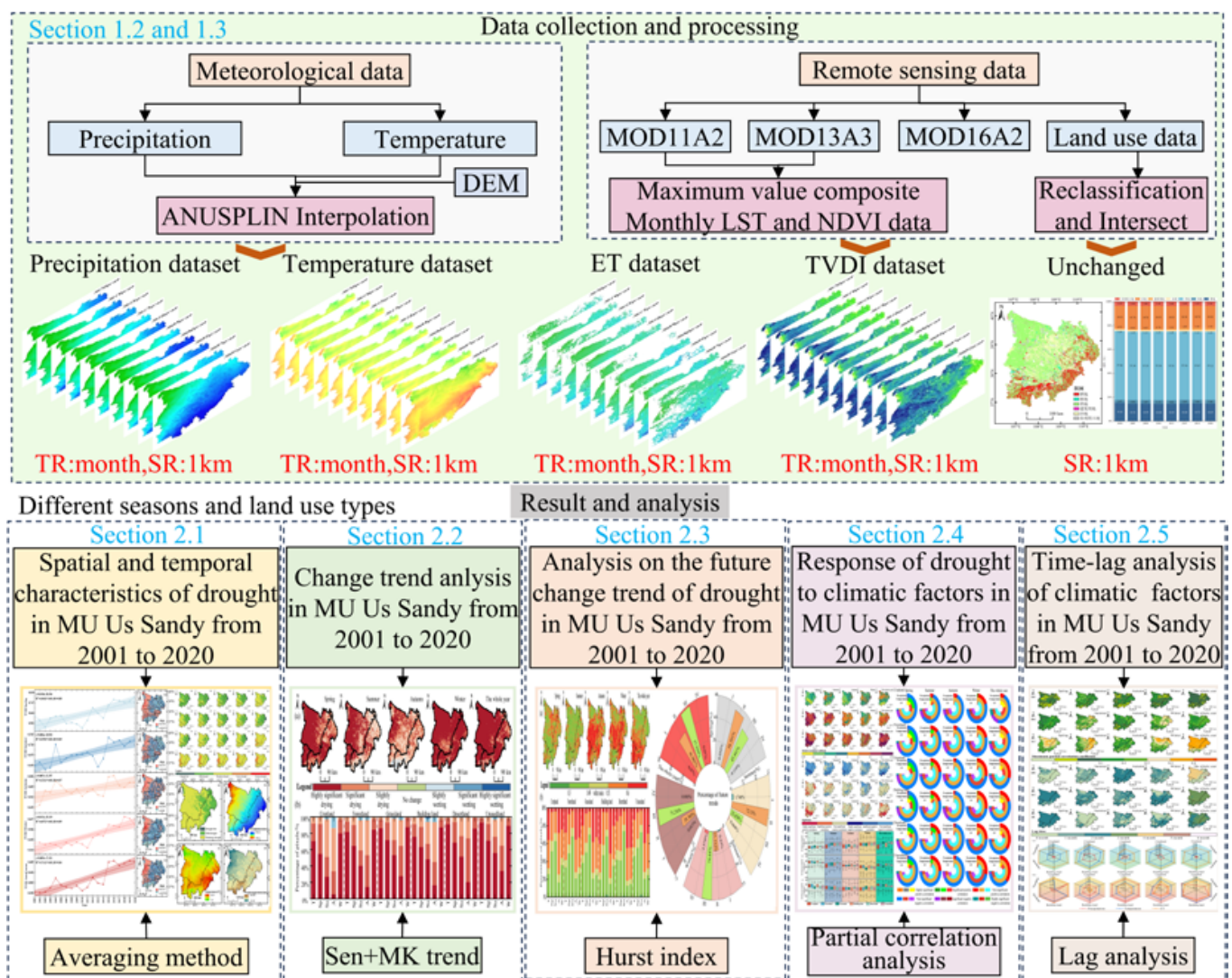


Figure 3. The technical flowchart.

2.3.1. TVDI

Sandholt et al. [19] discovered that the eigenspace among TS and NDVI had a series of soil moisture contours and that the slopes between the two were negatively correlated with the crop moisture index. This depends on the study of triangular distribution characteristics of scatter graphs of NDVI and Ts [26,27]. In order to represent the severity of the drought, TVDI was created utilizing this common connection. Below is the formula:

$$TVDI = (P_S - P_{Smin}) / (P_{Smax} - P_{Smin}) \quad (1)$$

where P_{Smin} is the smallest surface temperature at the equivalent $NDVI$ value for the wet side, P_{Smax} is the greatest surface temperature at the equivalent $NDVI$ value for the dry side, and PS is the recorded surface temperature in each pixel. Formula relating to wet and dry sides are obtained by linearly fitting all image elements with the same $NDVI$ values and corresponding LST maxima and minima:

$$\begin{aligned} P_{Smax} &= d_1 + g_1 \times NDVI \\ P_{Smin} &= d_2 + g_2 \times NDVI \end{aligned} \tag{2}$$

where λ indicates the $TVDI$ change tendency, Y_m, Y_n is the corresponding $TVDI$ value for m, n year, m, n indicates the duration order, and median is a median function. $TVDI$ exhibits a growing trend when $\lambda > 0$ and a falling trend otherwise and is used in conjunction with Mann–Kendall to assess the trend’s significance; the significance level α is taken as 0.05 and 0.01, respectively. Table 1 displays the trend’s precise division.

Table 1. Division for drought change trend altering MUSL.

λ	F	Trending Traits
$\lambda > 0$	$2.58 < F$	Highly significant drying
	$1.96 < F \leq 2.58$	Significant drying
	$F \leq 1.96$	Slightly drying
$\lambda = 0$	F	No change
$\lambda < 0$	$2.58 < F$	Highly significant wetting
	$1.96 < F \leq 2.58$	Significant wetting
	$F \leq 1.96$	Slightly wetting

For $TVDI$, drought grade classification adheres to [28] classification requirements for $TVDI$, which are provided in Table 2.

Table 2. $TVDI$ drought classification.

$TVDI$	0~0.46	0.46~0.57	0.57~0.76	0.76~0.86	0.86~1
Drought grade	Drought free	Mild drought	Moderate drought	Severe drought	Extreme drought

2.3.2. $TVDI$ Trend Evaluation of Change

This Sen slope approach was employed to examine the twenty-year trend for $TVDI$ variations in MUSL. The Mann-Kendall test was used to further evaluate the relevance of the Sen trend evaluation results. The formula for computing Sen is [29,30]:

$$\lambda = median\left(\frac{Y_n - Y_m}{n - m}\right), \forall n > m \tag{3}$$

where λ indicates the $TVDI$ change tendency, Y_m, Y_n is the corresponding $TVDI$ value for m, n year, m, n indicates the duration order, and median is a median function. $TVDI$ exhibits a growing trend when $\lambda > 0$ and a falling trend otherwise and is used in conjunction with Mann–Kendall to assess the trend’s significance; the significance level α is taken as 0.05, 0.01, respectively. Table 1 displays the trend’s precise division.

2.3.3. Hurst Exponent

Predicting future trends of drought in MUSL utilizing the Hurst exponent. A quantitative measure of time-series data over time, the autocorrelation that is useful for forecasting potential patterns is the Hurst exponent [31]. The Hurst value range is [0, 1], where Hurst = 0.5 means there is no process, as it is white noise; in this study, there are no pixels with Hurst = 0.5 in four seasons and the whole year round. Therefore, in order to draw

a clear boundary between white noise and non-white noise, based on the actual distribution characteristics of the data, statistical fluctuations, and measurement errors, 0.5 is used as the center, expanded to 0.01 on both sides, respectively, making the prediction results more reliable and intuitive; $0 < \text{Hurst} < 0.5$ suggests that the TVDI has an ant continuity series, meaning the projected pattern is the opposite from the past; and $0.5 < \text{Hurst} < 1$ indicates that the later years pattern corresponds in past results.

2.3.4. Partial Correlation Analysis and Lag Analysis

A partially correlated analysis and lag study examined the consequence of seasonal precipitation and temperature with ET for TVDI at different scales and TVDI's lag time on the three variables. The partially correlating coefficient equation is [32].

$$r_{ab.cd} = \frac{r_{ab.c} - r_{ad.c}r_{bd.c}}{\sqrt{(1 - r_{ad.c}^2)(1 - r_{bd.c}^2)}} \quad (4)$$

where a is TVDI; b is precipitation; c is temperature; d is ET; $r_{ab.c}$ represents the partial coherence coefficient that controls temperature TVDI with precipitation; $r_{ad.c}$ is with ET; $r_{bd.c}$ is precipitation; and $r_{ab.cd}$ is ET and temperature. Using analogies, the test of association was used to determine the partially correlated coefficient significance.

First, the partially correlated coefficients during TVDI with temperature, precipitation, and ET are computed for the current month, one month ahead, two months ahead, and six months ahead. Next, a maximum number of the corresponding image pixels' partial correlation at various scales is synthesized; an absolute number is taken to obtain the greatest partial correlation coefficients and their corresponding lag times. These are the fundamental steps of the lag analysis. Below is the expression [33]:

$$S = \max\{|R_0, R_1, R_2, \dots, R_{n-1}, R_n|\} \quad (5)$$

The greatest partial correlation value is S , and its lag time is n . The partial correlation values of TVDI are $R_0, R_1, R_2, \dots, R_{n-1}$, and R_n for the current month, 1 month forward, 2 months forward, and n months forward, respectively. When $R = R_n$, the lag time is n months. In this study, the seasonal division scale is based on 3 months; that is, the seasonal scale only calculates the partial correlation coefficient forwarded to 2 months, and the whole year scale calculates the partial correlation coefficient to 6 months forward.

3. Results

3.1. Drought Shifts through MUSL: Temporal and Spatial Features

Computing the temporal and geographical features for TVDI from MUSL during the previous 20 years using the mean value approach (Figure 4). With a constant rate of increase of $0.009/a$, the TVDI for the entire year exhibits a notable rising trend. The mild and moderate drought conditions are represented by the TVDI, centered in the range of 0.53 to 0.70. Moreover, the ways that distinct seasons alter things are distinct: the highest amount of drought occurs in the spring, with the average value basically concentrated between 0.54 and 0.80. In 2010, the TVDI value was significantly lower than other years, with a TVDI value of 0.54. In 2016, the TVDI was significantly higher than in other years and reached the maximum value of 0.80, which is a severe drought year. Winter is the season with the smallest degree of drought and the largest fluctuation, with TVDI values ranging from 0.38 to 0.66, and its abrupt change point occurred in 2012 and 2016 when it shifted from drought-free to mild drought to moderate drought. The rate of increase of TVDI in summer was the smallest in all seasons (growth rate = $0.006/a$, $R^2 = 0.539$), mainly distributed in Ejin Horo Banner, Shenmu County, Jingbian County, and southern Dingbian County, showing discontinuities in 2005 and 2013. Conversely, the greatest rate of increase in TVDI (growth rate = $0.013/a$, $R^2 = 0.697$) was observed in winter, primarily across the western portion of the Otog Banner and Otog Front Banner. Overall, 2015 was a year of abrupt change in TVDI.

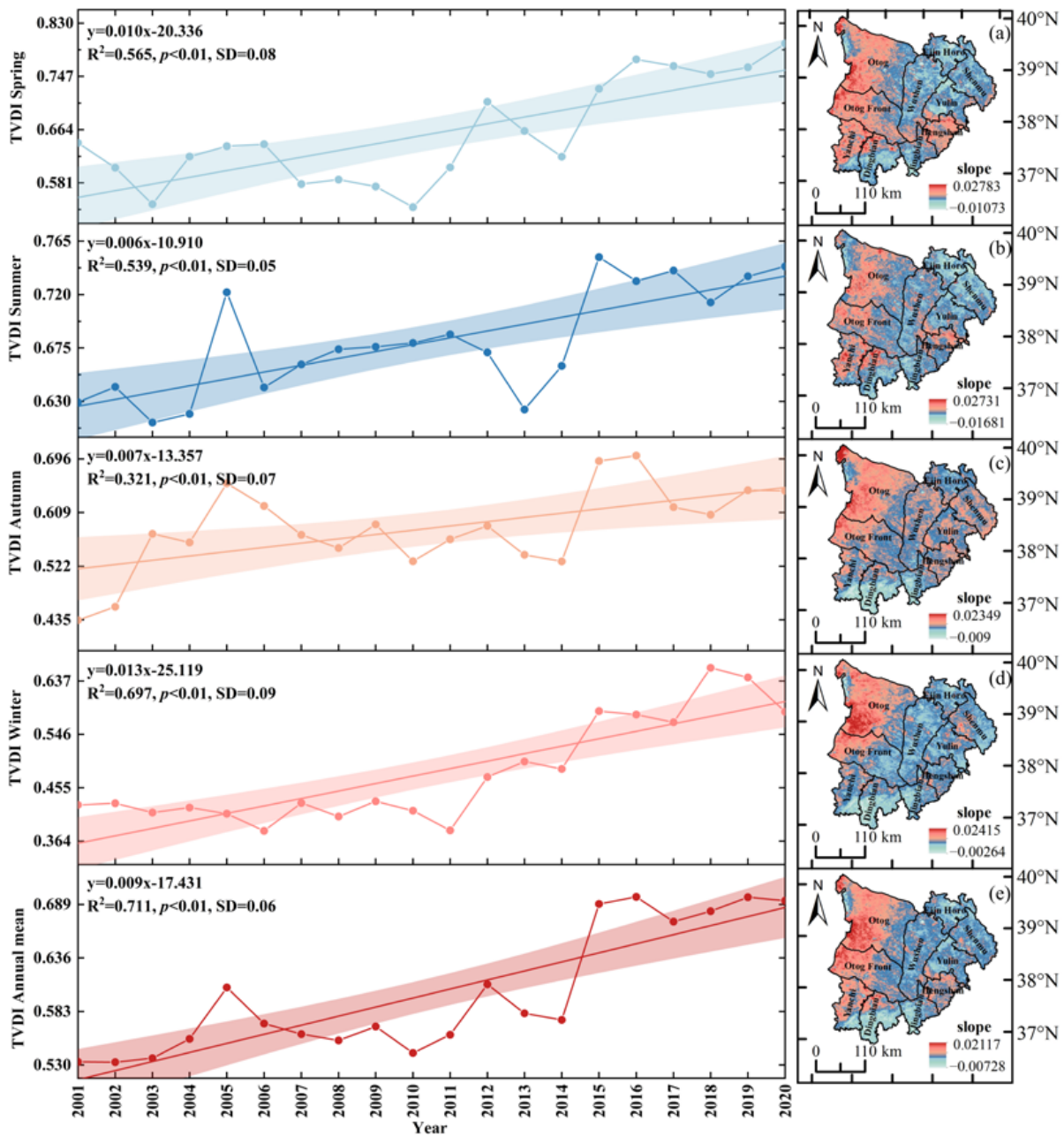


Figure 4. Geographical and temporal TVDI trends in MUSL seasons. (a) Spring, (b) summer, (c) autumn, (d) winter, (e) annual mean.

Figure 5 depicts the geographic distribution of drought classes throughout MUSL between 2001 and 2020. The west-to-east saw a slow improvement in the drought. In the northwest of Otog Banner and Otog Front Banner in Inner Mongolia, severe and intermittent droughts first appeared in 2015 and 2016, respectively. These droughts thereafter displayed an increasing tendency, with Otog Front Banner indicating the most noticeable rise. In 2019, the severe drought and extreme drought areas reached the largest areas, accounting for 18.3% and 0.1%, respectively. The locations with the least amount of drought between 2001 and 2014 were the eastern half of the county, the southeast portion of Yulin County, the north-central region of Wushen Banner, and Ejin Horo Banner. From Figure 6, the mean annual TVDI in MUSL is 0.6, indicating moderate drought (71.9%), with most of it in Yanchi, Dingbian, and the Ordos Plateau throughout the middle and west sections. Drought-free and mild drought are also the main types of droughts in the MUSL, which are

primarily found in Shaanxi and certain areas of Inner Mongolia, with the Ordos Plateau in the middle and western region of the MUSL, Yanchi County in Ningxia, and Dingbian County in Shaanxi accounting for 71.9% of the area experiencing moderate drought.

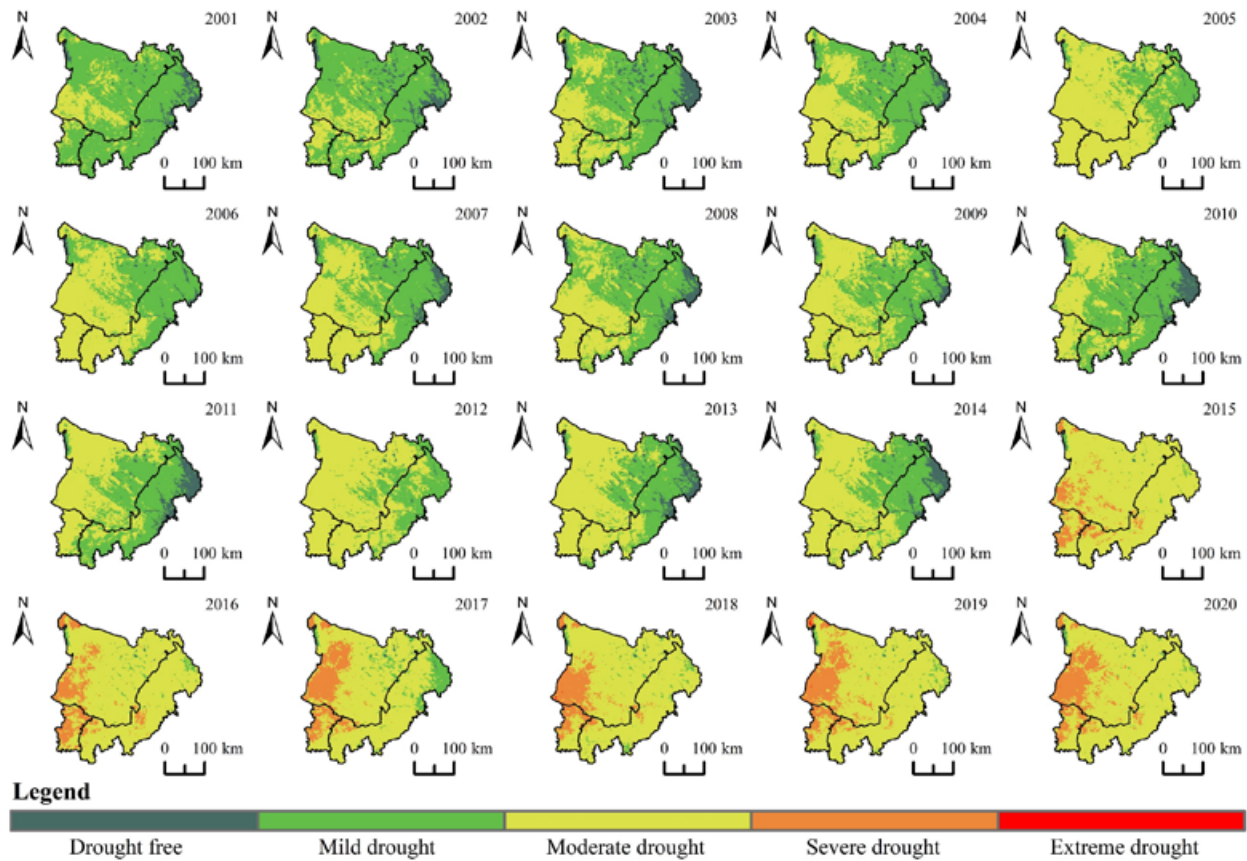


Figure 5. Location of MUSL drought grade from 2001 to 2020.

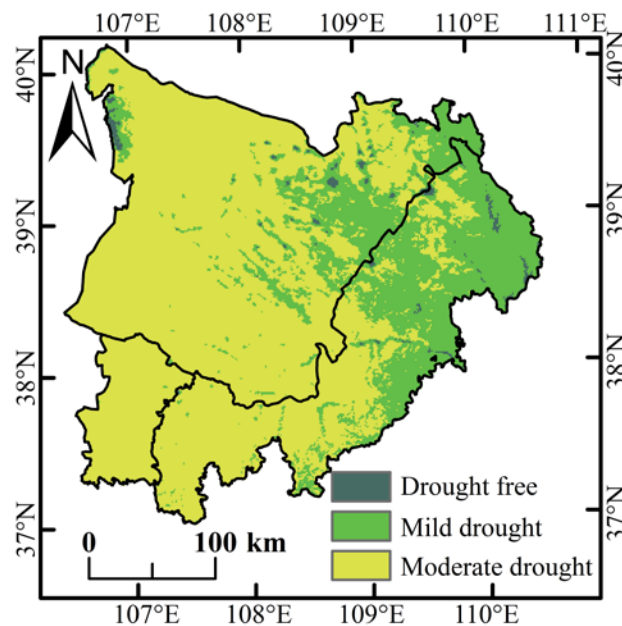


Figure 6. Mean annual TVDI in MUSL (2001–2020).

3.2. Trend Analysis of TVDI Changes in MUSL

Figure 7 shows that highly significant drying dominated in spring, summer, and winter (Z average = 2.95) and throughout the whole year ($Z = 3.47$). In spring, 67.3% of the highly significant drying zones are located in Yanchi County, Hengshan County, Otog Banner, and Otog Front Banner, increasing to 83.9% for the whole year. Slight drying in summer increased by 21.6%, mainly in the transformation of Wushen Banner and the northeastern and southern parts of MUSL. In autumn ($Z = 1.99$), 38.5% of the pixels were dominated by a significant drying trend, with 4.4% showing moist varieties in Yanchi County's southern region. Throughout the whole year, the change trend types of the six land types were dominated by highly significant drying—in descending order, unused land (93%), desert land (91%), grassland (85.7%), forestland (81.7%), building land (75.7%), and cropland (70.4%). The number of significantly dry pixels in spring was essentially the same across different land types, with percentages exceeding 20%. Summer was dominated by highly significant drying except for cropland, and the statistics for pixels showing slight drying in summer and autumn were broadly similar except for building land. The proportion of pixels in slightly dry areas of building land in autumn was 48.7%, significantly higher than other types. The distribution of pixel types in winter was more similar to that of the whole year, with over 99.7% of all types experiencing dry conditions ($p < 0.05$).

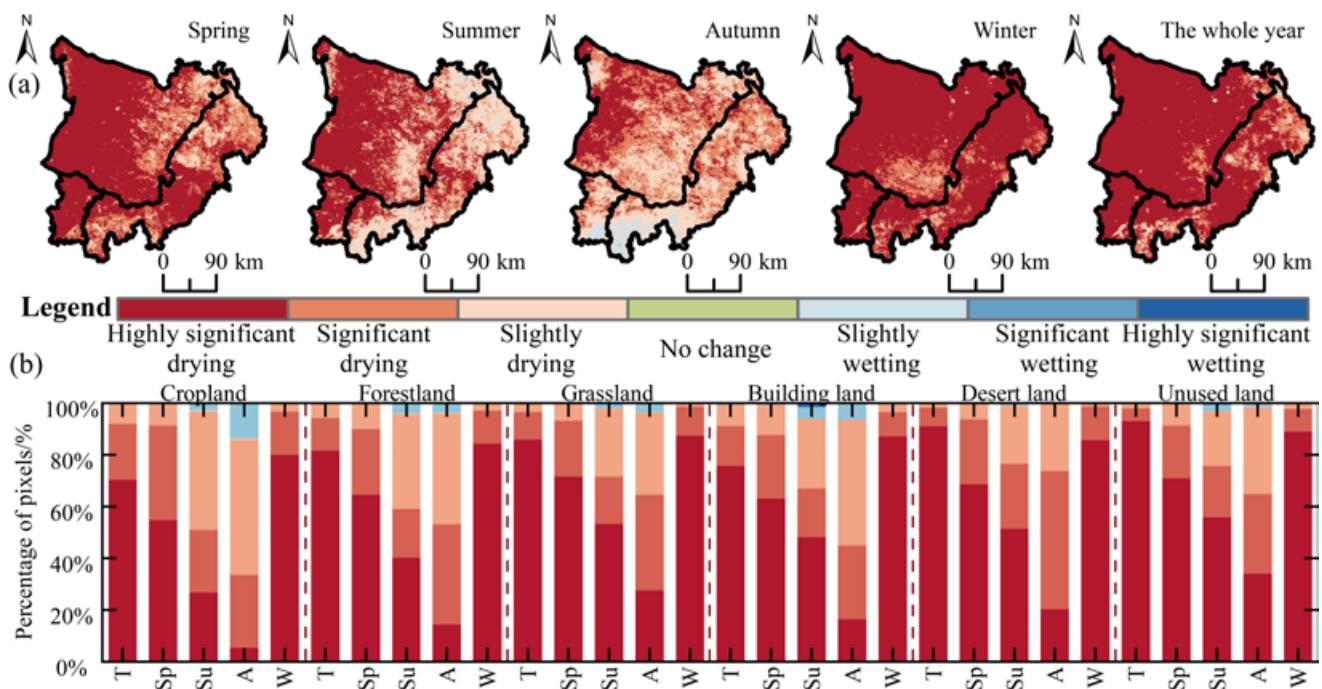


Figure 7. (a) Types of trends in drought changes and (b) trends in the significance for various utilizing land categories in MUSL (2001–2020). (T) The whole year; (Sp) spring; (Su) summer; (A) autumn; (W) winter.

3.3. Analysis of Future Continuing Trends in TVDI in MUSL

As shown in Figure 8, the Hurst exponent of the four seasons and the whole year in the MUSL ranged from 0.16 (summer) to 0.92 (winter). The averages for summer, fall, and winter were 0.45, 0.57, and 0.56, respectively, indicating that summer was mainly characterized by anti-persistence, while autumn and winter exhibited positive persistence. TVDI time series in spring and throughout the year appear close to white noise, suggesting that temporal and geographical changes in drought during spring and the entire year are largely random. The lowest value (0.36 in summer) and the highest value (0.73 in autumn and the whole year) of the Hurst exponent are both located in Yanchi County. This can be attributed to the area's location within the agro-pastoral ecotone, where increased

agricultural irrigation during summer, coupled with high temperatures leading to heightened vegetation evapotranspiration and inadequate precipitation, results in decreased soil moisture content and deteriorating vegetation development, thus exhibiting poor drought persistence. Conversely, the warm and humid climate in autumn facilitates vegetation recovery, leading to sustainable drought persistence. The Hurst exponent values for each land use type are concentrated above 0.51 in autumn and winter. Autumn and winter exhibit a significantly higher number of pixels with favorable relationships compared to spring and summer, with the proportion of pixels displaying negative relationships in autumn being less than 20%, significantly lower than the other three seasons and the entire year. The percentage of pixels for all land types with a Hurst exponent greater than 0.6 shows a pattern of increase, decrease, and subsequent increase from summer to winter, peaking in fall, indicating a progression from a small to a large percentage of strong positive, persistent pixels: autumn > winter > spring > summer. Forest grassland and unused land exhibit reverse persistence throughout the year, spring, and summer, while the proportion of pixels with Hurst exponent greater than 0.6 for cropland and building land in the entire year exceeds 36%.

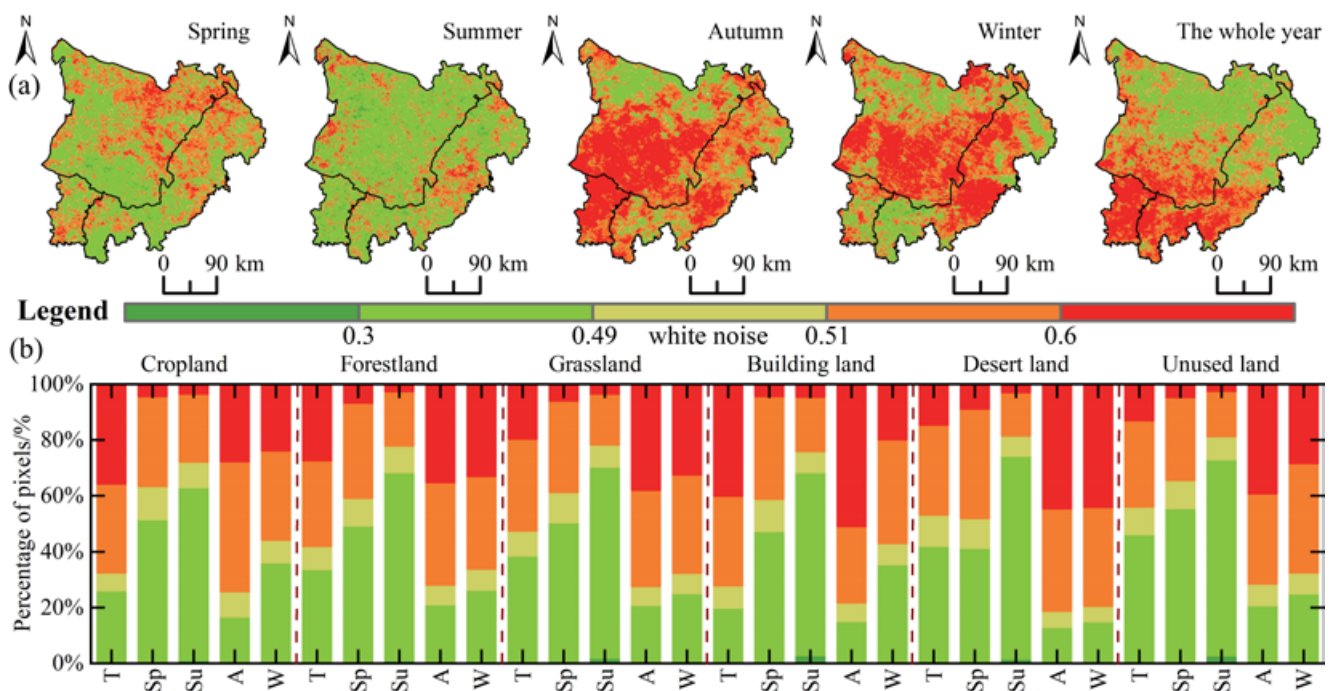


Figure 8. (a) Spatial Hurst exponent in different seasons and (b) percentage of Hurst exponent pixels for different land use types in MUSL (2001–2020). (T) The whole year; (Sp) spring; (Su) summer; (A) autumn; (W) winter.

To establish its inter-annual and seasonal change trend distribution of future drought in MUSL, the Hurst exponent is combined with a slope spatial change pattern mapping (Figure 9a). Annual and seasonal TVDI in MUSL are expected to mostly transition from dry to wet conditions and continual drying, with drought alleviation concentrated in central Ordos and Shenmu City. The springtime transition zone, primarily occurring in the middle of Otog Banner, Otog Front Banner, along with the surrounding counties of Dingbian and Jingbian, constitutes 54.39% of the whole; regional drought is projected to improve by 72.13% in summer, with fall and winter showing similar trends except for persistent wetting in the southeast for Yanchi District and the southern portion of Dingbian District.

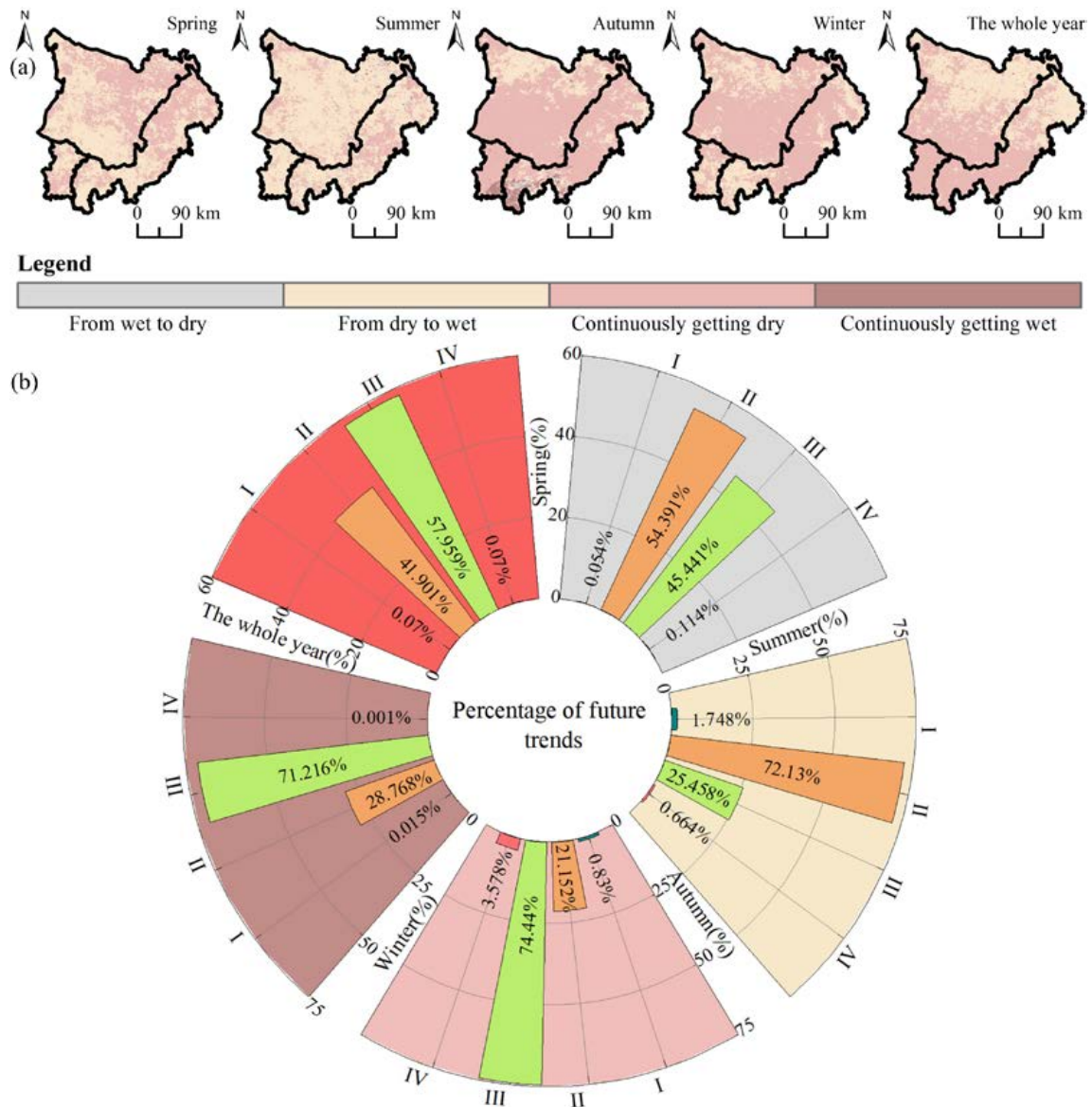


Figure 9. (a,b) Future trends in drought and percentage of future trends in MUSL. (I) From wet to dry. (II) From dry to wet. (III) Continuously becoming dry. (IV) Continuously becoming wet.

3.4. Response of Drought to Changes in Temperature, Precipitation, and ET

Figure 10 illustrates the insignificant negative correlation between TVDI and precipitation across the whole year, accounting for 63.4%, primarily observed in southern Shaanxi with higher altitudes and southeastern Yanchi County. The non-significant positive correlations with temperature and ET were 86.4% and 58%, respectively, with the absolute values of the average partial coefficients ranging from largest to smallest as follows: ET, 0.43; temperature, 0.15; and precipitation, 0.11. In spring, TVDI and temperature exhibited slightly higher mean partial correlation values ($r_1 = -0.33$, $r_2 = 0.39$, $r_3 = 0.37$) than precipitation and ET. Shenmu County, Yanchi County, and northern Dingbian County accounted for 24.6% of the significant positive correlation. In summer and autumn, TVDI mostly showed non-significant negative correlations with precipitation and non-significant positive correlations with temperature and evapotranspiration. The relative values of precipitation and TVDI in autumn ranged between -0.74 and -0.84 , with a high average partial coefficient (-0.28). In winter, the mean partial correlation values between TVDI and ET were larger than those of precipitation and temperature. The correlations ranged from negative to positive to negative from west to east, with non-significant positive cor-

relations pre-dominating, while some areas of Wushen Banner showed highly significant positive correlations.

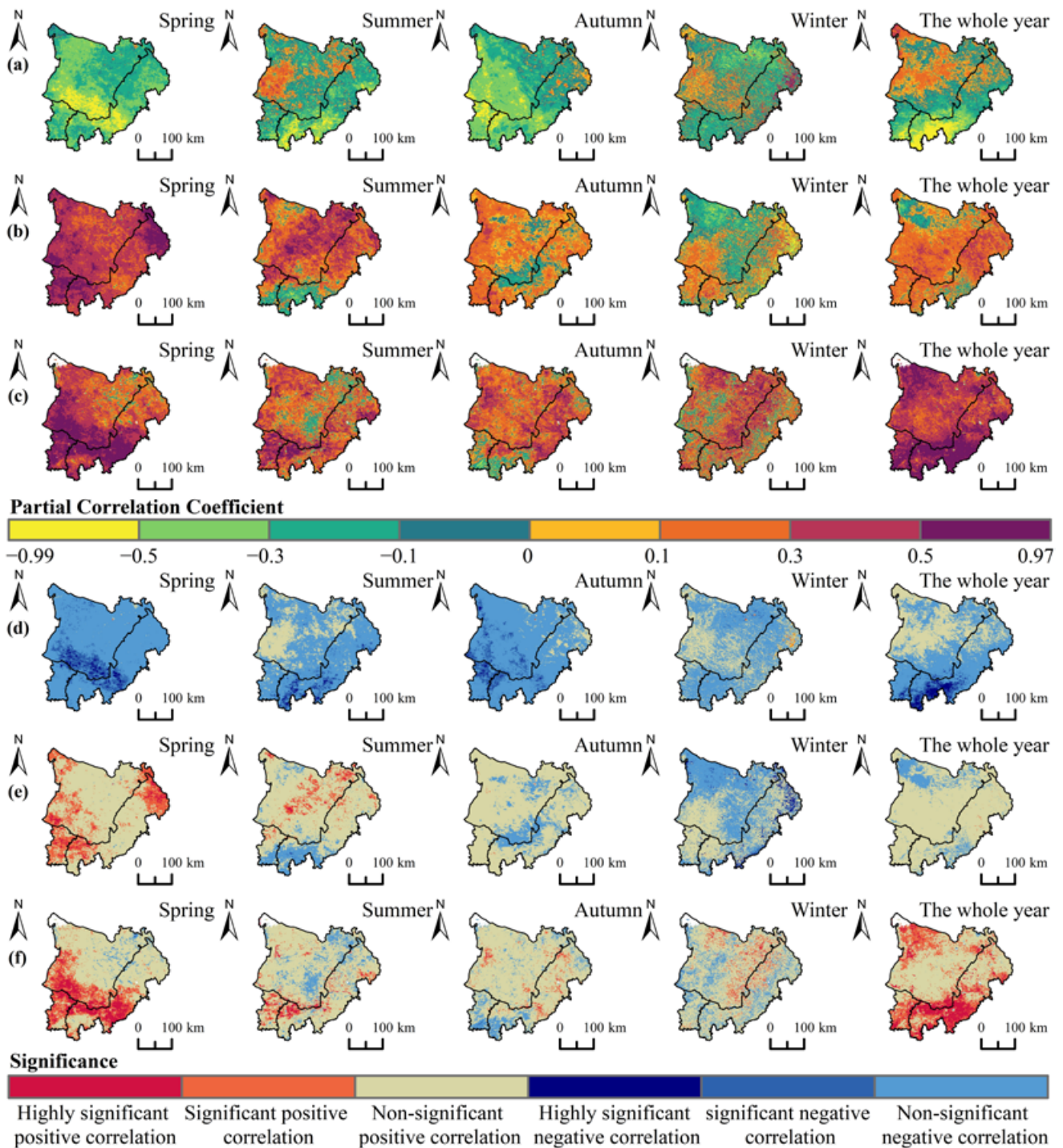


Figure 10. Spatial distribution of correlation coefficients and significance of TVDI with precipitation (a–d), temperature (b–e), and ET (c–f) bias in different seasons of MUSL (2001–2020).

Figures 11 and 12 depict the partial correlation values between spring precipitation and TVDI for the six land use types, primarily ranging from -0.44 to -0.18 , with over 80% exhibiting an insignificant negative correlation. Forestland exhibited a slightly more significant negative correlation than the other five types. In summer, compared to spring, the partial correlation coefficients were considerably lower and more dispersed, indicating

that TVDI responded more strongly to precipitation in spring than in summer. The pattern of partial correlation values in fall mirrored that of summer, except for forestland, which showed roughly an 18% significant negative correlation with building land. Winter seasons were characterized by predominantly non-significant negative correlations, with partial correlation coefficients for grassland, desert land, and unused land closer to those of summer, while all others were lower than the other three seasons. Non-significant negative correlation pre-dominated throughout the whole year, except for building land and unused land. Spring TVDI exhibited the strongest partial correlation values with temperature among the six categories, while summer desert land showed greater partial correlation values than the other five types. Correlation coefficients of different types in autumn were concentrated above 0.01, with more stable fluctuations than in summer. In winter, the correlation between different land types across seasons except grassland was minimal, with the lowest value of 0.02 observed for the correlation coefficient between grassland and temperature over the course of the year, indicating that grassland in winter and the whole year is not sensitive to temperature. Partial correlation coefficients between TVDI and ET for all land types except desert land in autumn exhibited a decrease followed by an increase throughout all seasons and the whole year, with trough and peak positions in autumn and the whole year, respectively. The whole year averaged higher correlation coefficients across various land types than the four seasons, with less variability observed among the same land use types. TVDI and ET exhibited an insignificant positive association in both seasons and the whole year.

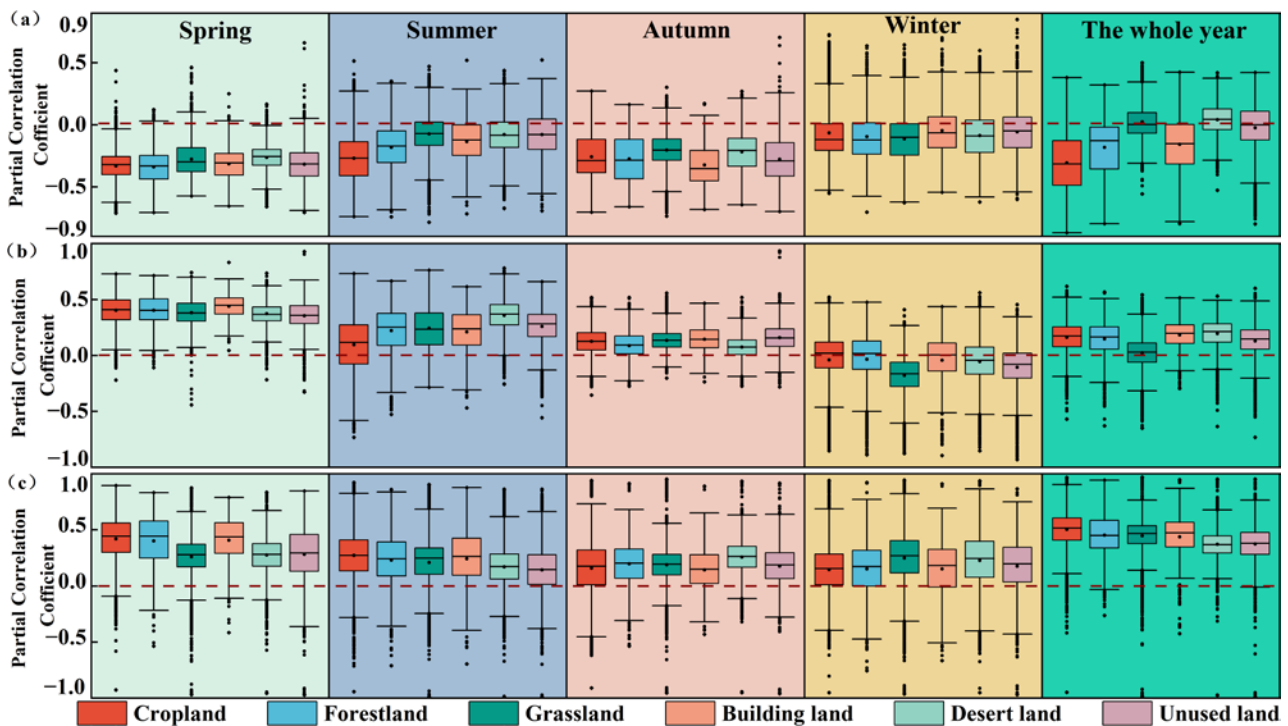


Figure 11. TVDI partial coefficients associated with (a) precipitation, (b) temperature, and (c) ET across various land utilization categories in different seasons in MUSL from 2001 to 2020.

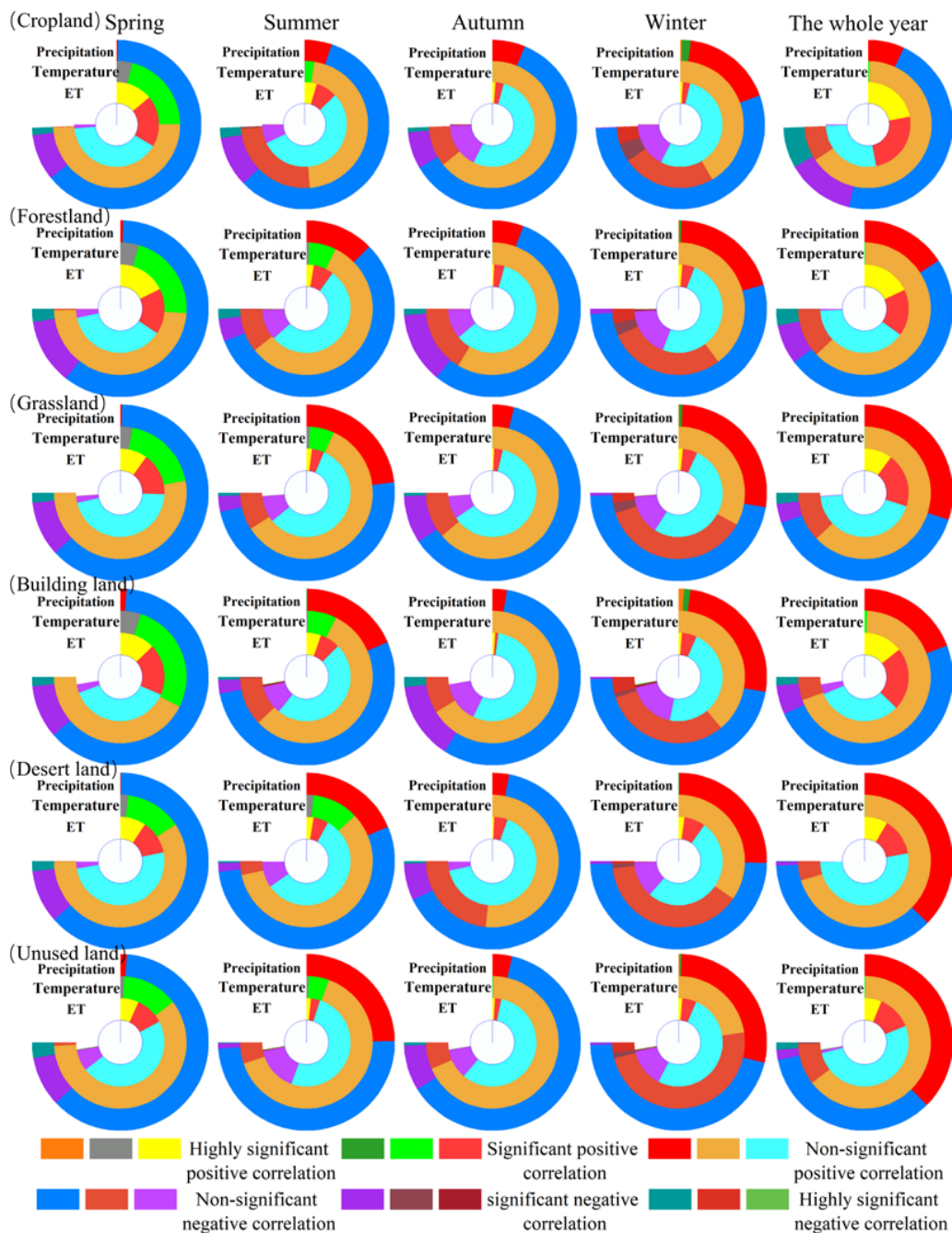


Figure 12. The significant pixel statistics of the correlation between TVDI and precipitation, temperature, and ET in diverse types of land use and seasons in MUSL. Each legend represents, from left to right, the statistics of significant pixels between TVDI and precipitation, temperature, and evapotranspiration.

3.5. Lag Analysis of Temperature, Precipitation, and ET in Annual Drought and Different Seasons

Figure 13a,c reveal that summer precipitation and TVDI exhibited the highest mean partial correlation value (0.13), with higher values observed in the northeast and central sections compared to the northwest and south, particularly at higher altitudes in Otog Banner and the southern half of Shanxi. Temperature and TVDI displayed the largest mean partial correlation value in winter (0.25), with 30% of the research region exhibiting values above 0.3, primarily in the northeast. The correlation between ET and TVDI had the highest annual mean partial correlation value (0.48), with strong spatial patterns observed in the middle and northern regions, while the south showed a lower correlation. The region

with the highest partial correlation value between 0.4 and 0.6 encompassed 79% of the area. As indicated in Figure 13d,f, the greatest effect of precipitation was observed in spring (0.3 months), with the minimum effect in autumn. The greatest effect of temperature occurred in autumn (1.2 months), while the minimum occurred at emergence. For ET, the greatest effect was in summer (0.3 months), with the minimum in spring, suggesting that TVDI in spring is more sensitive to precipitation but responds slowly to temperature (1.8 months) and ET (2 months). The standard deviation of TVDI lag time for temperature (0.8) and ET (1.1) was greater in autumn than in spring (0.4). The average lag times of TVDI to the three factors on an annual scale were 2.37 (with a standard deviation of 2.04 months), 2.97 (with a standard deviation of 0.37 months), and 2.58 (with a standard deviation of 0.75 months), respectively, indicating that the lagged response of TVDI to precipitation is more complex. About 42% of the regions showed no observed lag of TVDI to precipitation, while 50% of the regions exhibited a 4-month lag. Only 0.2% of regions had no lag in TVDI for temperature, with 93% showing a 3-month lag. In response to ET, 41% and 53% of regional TVDI exhibited 2-month and 3-month lags, respectively. The 6-month lag region was primarily located in the southern portion of Jingbian County, accounting for about 2% of the entire area, with sporadic distribution in its northern section.

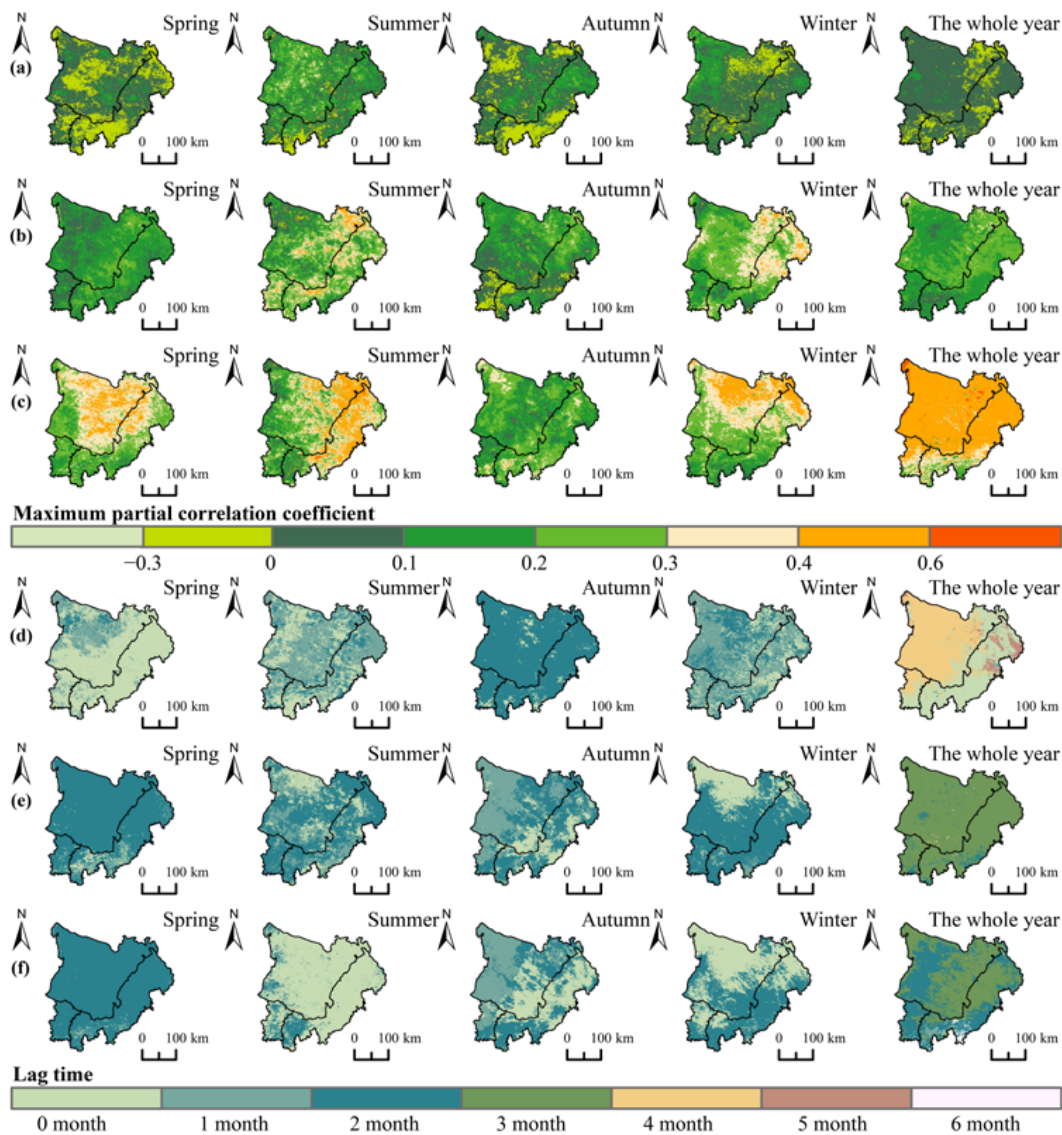


Figure 13. (a–c) TVDI greatest biased correlation value and (d–f) lag times regarding precipitation, temperature, and the ET through MUSL (2001–2020).

The greatest biased correlation values (between 0.16 and 0.51) of ET with various land use categories are much bigger than those of temperature and precipitation (Figure 14a). ET has the strongest impact on desert land in the spring and the whole year, while the weakest impact is on cropland. Figure 14b indicates that several land utilization patterns exhibit shorter seasonal lag times to precipitation in summer and fall, with average lag times ranging between 0.1 and 0.9 months. Forestland has the fastest response to temperature in spring, and various land use types are more sensitive to ET in the rest of the seasons, with the average lag time ranging between 0.1 and 1.2 months; all land use types were slowest responsive to temperature in summer and winter, while spring and autumn have the weakest sensitivity to ET and precipitation, respectively. On annual scale, cropland, forestland, building land, and desert land responded fastest to precipitation, and grassland and unused land responded fastest to ET; the response time to precipitation in descending order was desert land (2.7 months), building land (2.3 months), forestland (1.7 months), and cropland (1 month), indicating that cropland was the fastest to respond to precipitation, while desert land was the slowest; the response time to ET in descending order was grassland (2.5 months) and unused land (2.4 months), and then unused land had the fastest response time to ET. With the exception of abandoned land, which has an average lag time of three months (0.18 SD) to temperature, other land use types have the largest lag times. For every type of land, the temperature response time was longer than ET.

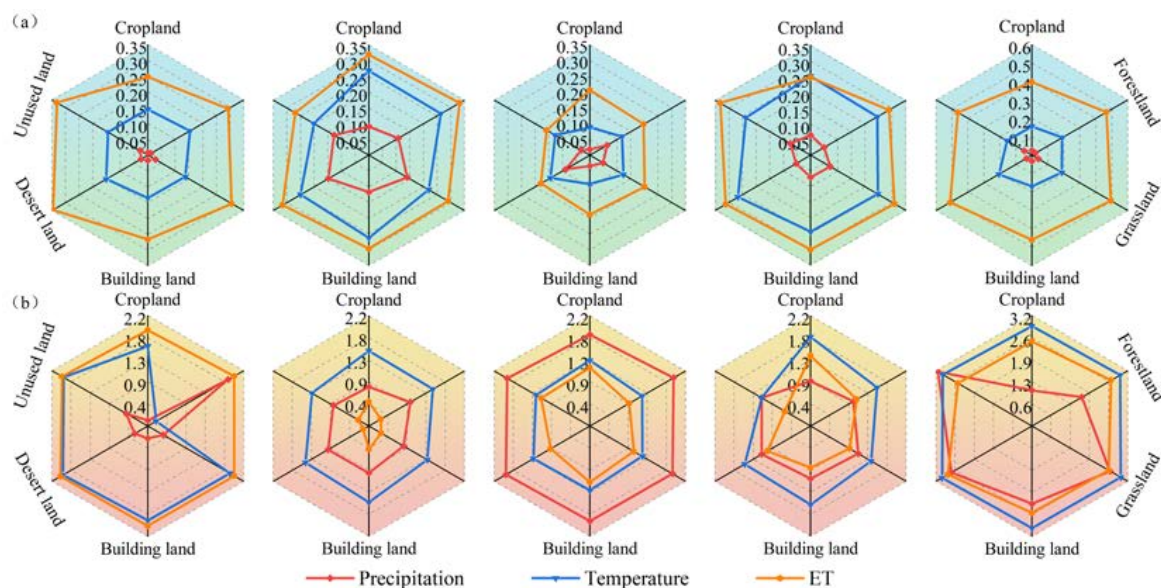


Figure 14. (a) Maximum partial correlation coefficient and (b) lag times of TVDI with precipitation, temperature, and ET for different land use types.

4. Discussion

By studying the trend of drought change in MUSL from 2001 to 2020, it was found that the western part was mainly dominated by an increasing trend (mainly distributed in Otog Front Banner), and the eastern part of the TVDI was dominated by a decreasing rate. These findings were consistent with the findings of [22] yet differed from those of Lian et al. [10]. On the one hand, it is difficult to determine the precise level of drought at broad scales or in areas with few meteorological stations due to the difficulty of calculating the SPEI index for studying droughts using data from a limited number of meteorological stations. On the other hand, this is due to the utilization of various drought assessment parameters as a foundation for classifying the identical metric into drought grades, the duration length of the investigation, and division boundaries. These factors can lead to contradictory conclusions.

Over the previous 20 years, a highly significant drying trend has dominated the MUSL TVDI. However, in the next time frame, the severity of the drought in Shenmu City, Shaanxi province, and central Ordos diminished, especially in summer, when 72.13% of the area will change from dry to wet. This occurrence will mostly be owing to the MUSL program that converted farms back to forests while grasslands and the warmer and wetter climate have increased vegetation cover to alleviate drought [34]. Moreover, the climate of the continually drying zone through the southern portion of MUSL is mostly cropland, with high altitudes and specific salts in the parent material of the soil, all of which have a severe negative influence on a boost of plants [35], and 58.7% of the plants in MUSL “turned green” as a result of the rise in CO₂, which led to an increase in NPP, an increase in ET [36], a decrease in soil moisture, and an intensification of drought [37]. The most severe droughts occur in the spring, when temperatures rise quickly, and precipitation levels drop as a result of shifting monsoon patterns [38,39] and the notable rise in the number of days with high temperatures [40]; further, the investigation’s results demonstrate an excellent relationship between the multi-year TVDI allocation features and the geographic distribution of annual mean precipitation; Moreover, El Niño–Southern Oscillation (ENSO) and drought are closely linked [41], and the El Niño phenomenon is thought to possess a bigger influence on dryness throughout MUSL. [10]. Vegetation restoration from 2001 to 2010 increased ET by 51 mm in MUSL [42], which can then cause the soil to dry up and prevent vegetation development, particularly in grasslands, resulting in a longer-lasting drought.

Having pointed out that dryness affects plants with a time lag [43], globally, drought usually has a lag time of one month for 88.37% of grasslands [44]. Currently, grassland makes up 58.71% of the MUSL due to vegetation restoration; however, on the investigated dimension, vegetation reacts to climate variability 1–2 months later than it does in adjacent regions [45]. Thus, while drought has an indirect lag effect on climate, does drought also have a direct lag effect on the weather elements? Therefore, to seek ways to enhance our comprehension of climate variability and the dynamics of drought feedback, this paper explores, in detail, the lagged relationship of TVDI on precipitation, temperature, and ET for different land use types at different scales. The results of this paper show that annual scale TVDI responds more quickly to precipitation than ET and temperature because the effects of temperature and ET on drought need to accumulate over a period of time to have a large impact on the current drought. Exploring the differences in the lag time of drought to climate elements for various land uses, this has to do with how various kinds of land usage are distributed and what makes them unique, such as soil type [46,47]. There is a significant increase in precipitation with elevation of the terrain on precipitation [48]. Grassland, building land, cropland, forestland, unused land, and desert land are distributed from high to low elevations. Grassland has a low sensitivity to precipitation, which may be due to the fact that drought sensitivity to precipitation decreases significantly when reaching a certain elevation range. Different soil textures have different sensitivities to precipitation and ET. For example, the difference in soil texture leads to different sensitivity to rainfall and evapotranspiration. For example, soils with high sediment concentration have lower water storage capacity and higher surface evaporation rate, while soils with high clay content have lower surface evaporation due to their stronger water retention [49]. The soil on the underlying surface of MUSL is mainly composed of sand grains, and the content is 50–90% [50]; there is a large proportion of loamy soil on building land, forestland, and cropland, and a sizable fraction of sand grains on underused and arid terrain, that are essentially in line with the investigation’s findings.

5. Conclusions

- (1) From 2001 to 2020, TVDI (mean value 0.6) was greater for its west and smaller for its east. Drought severity varies by season, with the order being spring > summer > autumn > winter. Summer had the lowest growth rate (0.006/a, R² = 0.539), while winter exhibited the highest (0.013/a, R² = 0.697).

- (2) A significant drying trend dominated in autumn ($Z = 1.99$), and a highly significant drying trend prevailed in the remaining three seasons (Z average = 2.95) and the whole year ($Z = 3.47$). The minimum value (0.36 in summer) and maximum value (0.36 in autumn and the whole year) of the Hurst index are located in Yanchi County, and the future drought mitigation area is expected to be in central Ordos and Shenmu City. Spring and summer are mainly dry to wet, whereas autumn and winter are mainly continuous dry.
- (3) The TVDI of the whole year and the four seasons (-0.07) was mainly negatively correlated with precipitation. During spring, summer, and fall, TVDI exhibited a favorable correlation with temperature and ET, while in winter, it had an inverse relationship with temperature (-0.06) and a positive correlation with ET (0.18). TVDI was predominantly non-significantly negatively correlated with precipitation for all land use types in all seasons. Land use type and temperature were predominantly non-significantly positively correlated in spring, summer, autumn, and throughout the whole year. Different land types and ET were predominantly non-significantly positively correlated in all four seasons and throughout the whole year.
- (4) On the seasonal scale, spring TVDI was most sensitive to precipitation (0.3 months) and slow to respond to temperature (1.8 months) and ET (2 months). The standard deviation of the lag time of TVDI for temperature (0.8) and ET (1.1) was greater in autumn than in spring (0.4). Annually, precipitation was the most contributing element of cropland, forestland, building land, and desert land (2.6 months); ET has the strongest impact on grassland and unused land; desert land has the weakest sensitivity to temperature (3 months).

Author Contributions: Writing—original draft, F.W.; methodology, F.W., S.W. and H.W.; investigation, F.W.; funding acquisition, R.L.; validation, R.L.; resources, R.L. and Y.S.; project administration, R.L.; writing—review and editing, S.W.; formal analysis, H.W.; data curation, Y.S., Y.Z., J.Z. and J.Y. All authors have read and agreed to the published version of the manuscript.

Funding: The investigation was funded by the Natural Science Foundation of Inner Mongolia Autonomous Region (2022MS05044) and the National Natural Science Foundation of China (52269004).

Informed Consent Statement: Not applicable.

Data Availability Statement: The original contributions presented in the study are included in the article, further inquiries can be directed to the corresponding author.

Acknowledgments: The authors thanks the Inner Mongolia and National Natural Science Foundations for supporting this work.

Conflicts of Interest: The authors declare no conflicts of interest.

References

1. Liu, Y.; Huang, S.; Fang, W.; Ma, L.; Zheng, X.; Huang, Q. Propagation and dynamic change of meteorological drought to hydrological drought in different seasons. *J. Hydraul. Eng.* **2021**, *52*, 93–102. [\[CrossRef\]](#)
2. Gao, Y.; Markkanen, T.; Thum, T.; Aurela, M.; Lohila, A.; Mammarella, I.; Kämäräinen, M.; Hagemann, S.; Aalto, T. Assessing various drought indicators in representing summer drought in boreal forests in Finland. *Hydrol. Earth Syst. Sci.* **2016**, *20*, 175–191. [\[CrossRef\]](#)
3. Li, Y.; Cheng, W.; Zuo, W.; Zhang, L. Agricultural vulnerability to drought in China's agro-pastoral ecotone: A case study of Yulin City, Shaanxi Province. *Chin. Geogr. Sci.* **2023**, *33*, 934–945. [\[CrossRef\]](#)
4. Yuan, Y.; Ye, X.; Liu, T.; Li, X. Spatio-temporal Characteristics of Integrated Drought in Poyang Lake Basin Based on Multi-source Remote Sensing Data. *Res. Environ. Yangtze Basin.* **2024**, *33*, 214–227.
5. Chen, Y.; Sun, L.; Du, Y.; Han, W.; Hu, H. Progress and Prospect of Remote Sensing Monitoring on Agricultural Drought. *Remote Sens. Inf.* **2022**, *37*, 1–7. [\[CrossRef\]](#)
6. Liu, X.; Guan, M.; Li, X.; Gu, C. Progress in Bibliometric-based Remote Sensing Drought Monitoring Research. *J. Catastrophol.* **2023**, *39*, 1–14.
7. Wang, C.; Han, X.; Wang, H.; You, J. Responses of Vegetation in Mu Us Sandy Land to Climate Change from 1982 to 2020. *For. Grassl Resour Res.* **2023**, *137*, 80–89. [\[CrossRef\]](#)

8. Fang, X.; Liu, X.; Yue, D. Analysis of Climate Change Characteristics and Influencing Factors in Mu Us Sandy Land from 1960 to 2018. *Res. Soil Water Conserv.* **2022**, *29*, 163–169. [[CrossRef](#)]
9. Xu, Z.; Lu, H. Aeolian environmental change studies in the Mu Us Sandy Land, north-central China: Theory and recent progress. *Acta Geogr. Sin.* **2021**, *76*, 2203–2223. [[CrossRef](#)]
10. Lian, H.; Han, X.; Liu, Y.; Han, Y.; Yang, W.; Xiong, W. Study on spatiotemporal characteristics of atmospheric drought from 1981 to 2020 in the Mu Us Sandy Land of China based on SPEI index. *J. Desert Res.* **2022**, *42*, 71–80.
11. Shi, L.; Li, H.; Zhao, Y.; Ren, Y.; He, J.; Yu, F.; Hasi, E. Benefit evaluation of wind prevention and sand fixation under the combined measures of sand barrier in mobile dunes in Mu Us sandy land. *Arid Zone Res.* **2023**, *40*, 268–279. [[CrossRef](#)]
12. Zhou, X.; Wang, P.; Tansey, K.; Zhang, S.; Li, H.; Wang, L. Developing a fused vegetation temperature condition index for drought monitoring at field scales using Sentinel-2 and MODIS imagery. *Comput. Electron. Agric.* **2020**, *168*, 105144. [[CrossRef](#)]
13. Jackson, R.D.; Idso, S.; Reginato, R.; Pinter, P., Jr. Canopy temperature as a crop water stress indicator. *Water Resour. Res.* **1981**, *17*, 1133–1138. [[CrossRef](#)]
14. Liu, S.; Pan, X.; Yang, Y.; Yuan, J.; Yang, Z.; Wang, Z.; Xie, W.; Song, H. A Crop water stress index based on Remote Sensing methods for monitoring drought in an Arid area. *Remote Sens. Lett.* **2023**, *14*, 890–900. [[CrossRef](#)]
15. Tang, S.; Zhang, X.; Chen, N. Adaptability analysis of drought index in soil moisture monitoring. *Sci. Surv. Map.* **2021**, *46*, 114–119. [[CrossRef](#)]
16. Wei, W.; Yan, P.; Zhou, L.; Zhang, H.; Xie, B.; Zhou, J. A comprehensive drought index based on spatial principal component analysis and its application in northern China. *Environ. Monit. Assess.* **2024**, *196*, 193. [[CrossRef](#)]
17. Qin, Y. Comprehensive Drought Monitoring Based on SPEI and TVDI in Inner Mongolia, China. Master's Dissertation, Chengdu University of Technology, Chengdu, China, 2020. [[CrossRef](#)]
18. Zhao, G.; Li, X.; Li, B. An Overview on Agricultural Drought Monitoring Methods Based on Land Surface Temperature and Vegetation Index Feature Space. *Res. Soil. Water Conserv.* **2010**, *17*, 245–250.
19. Sandholt, I.; Rasmussen, K.; Andersen, J. A simple interpretation of the surface temperature/vegetation index space for assessment of surface moisture status. *Remote Sens. Environ.* **2002**, *79*, 213–224. [[CrossRef](#)]
20. Guo, Y.; Han, L.; Zhang, D.; Sun, G.; Fan, J.; Ren, X. The Factors Affecting the Quality of the Temperature Vegetation Dryness Index (TVDI) and the Spatial–Temporal Variations in Drought from 2011 to 2020 in Regions Affected by Climate Change. *Sustainability* **2023**, *15*, 11350. [[CrossRef](#)]
21. Luo, B.; Liu, X.; Guo, P. Remote sensing drought monitoring of Hetao irrigation area based on MODIS data. *J. China Agric. Univ.* **2020**, *25*, 44–54. [[CrossRef](#)]
22. Wang, Y.; Shi, H.; Jiang, Y.; Wu, Y.; Gao, Y.; Ding, C. Spatio-temporal Variation of Drought Characteristics and Its Influencing Factors in Loess Plateau Based on TVDI. *Trans. Chin. Soc. Agric. Mach.* **2023**, *54*, 184–195. [[CrossRef](#)]
23. Fan, L.; Geng, B.; Wang, J.; Chen, J. Temporal and Spatial Dynamics of Drought and Its Response to Climate Change in the Loess Plateau from 2001 to 2020. *Res. Soil Water Conserv.* **2022**, *29*, 183–191. [[CrossRef](#)]
24. Zhou, T.; Han, C.; Qiao, L.; Ren, C.; Wen, T.; Zhao, C. Seasonal dynamics of soil water content in the typical vegetation and its response to precipitation in a semi-arid area of Chinese Loess Plateau. *J. Arid Land* **2021**, *13*, 1015–1025. [[CrossRef](#)]
25. Zhao, J.; Zhang, X.; Liao, C.; Bao, H. TVDI based Soil Moisture from Remotely Sensed Data over Large Arid Areas. *Remote Sens. Technol. Appl.* **2011**, *26*, 742–750.
26. Carlson, T.; Gillies, R.; Perry, E. A method to make use of thermal infrared temperature and NDVI measurements to infer surface soil water content and fractional vegetation cover. *Remote Sens. Rev.* **1994**, *9*, 161–173. [[CrossRef](#)]
27. Price, J. Using spatial context in satellite data to infer regional scale evapotranspiration. *IEEE Trans. Geosci. Remote Sens.* **1990**, *28*, 940–948. [[CrossRef](#)]
28. Wu, L. Classification of drought grades based on temperature vegetation drought index using the MODIS data. *Res. Soil Water Conserv.* **2017**, *24*, 130–135+3. [[CrossRef](#)]
29. Hoaglin, D.; Mosteller, F.; Tukey, J. *Understanding Robust and Exploratory Data Analysis*; John Wiley & Sons: Hoboken, NJ, USA, 2000; Volume 76.
30. Zhao, N.; Zhao, Y.; Zou, H.; Bai, X.; Zhen, Z. Spatial and temporal trends and drivers of fractional vegetation cover in Heilongjiang Province, China during 1990–2020. *Chin. J. Appl. Ecol.* **2023**, *34*, 1320–1330. [[CrossRef](#)]
31. Long, Y.; Jiang, F.; Deng, M.; Wang, T.; Sun, H. Spatial-temporal changes and driving factors of eco-environmental quality in the Three-North region of China. *J. Arid Land* **2023**, *15*, 231–252. [[CrossRef](#)]
32. Wu, Y.; Yang, J.; Li, S.; Guo, C.; Yang, X.; Xu, Y.; Yue, F.; Peng, H.; Chen, Y.; Gu, L.; et al. NDVI-Based Vegetation Dynamics and Their Responses to Climate Change and Human Activities from 2000 to 2020 in Miaoling Karst Mountain Area, SW China. *Land* **2023**, *12*, 1267. [[CrossRef](#)]
33. Hua, Y.; Gao, R.; Ao, D. Temporal Lag of Desert Steppe Vegetation Growth Response to Climate Factors in Inner Mongolia. *J. Northwest For. Univ.* **2021**, *36*, 1–10.
34. Wang, X.; Song, J.; Xiao, Z.; Wang, J.; Hu, F. Desertification in the Mu Us Sandy Land in China: Response to climate change and human activity from 2000 to 2020. *Geogr. Sustain.* **2022**, *3*, 177–189. [[CrossRef](#)]
35. Liu, Q.; Zhang, Q.; Yan, Y.; Zhang, X.; Niu, J.; Svenning, J. Ecological restoration is the dominant driver of the recent reversal of desertification in the Mu Us Desert (China). *J. Clean. Prod.* **2020**, *268*, 122241. [[CrossRef](#)]

36. Yang, L.; Li, Y.; Fan, H.; Wang, Y. Temporal and spatial distribution and influencing factors of evapotranspiration in Mu Us Sandy Land. *J. Agric. Sci. Technol.* **2022**, *24*, 169–178. [[CrossRef](#)]
37. Li, C.; Fu, B.; Wang, S.; Stringer, L.C.; Wang, Y.; Li, Z.; Liu, Y.; Zhou, W. Drivers and impacts of changes in China’s drylands. *Nat. Rev. Earth Environ.* **2021**, *2*, 858–873. [[CrossRef](#)]
38. Li, J.; Guo, L.; Yang, M.; Zhao, G.; Wang, T. Climate warming hiatus and characteristics of air temperature and precipitation in Mu Us Sandy Land. *J. Water Resour. Water Eng.* **2022**, *33*, 72–80. [[CrossRef](#)]
39. Li, M.; Li, C. Temporal and spatial evolution characteristics of meteorological drought in the Loess Plateau from 1961 to 2020. *Pearl River.* **2023**, *44*, 1–10.
40. Deng, Z.; Zhang, Q.; Xu, J.; Chen, M.; Qin, S.; Zhang, S. Comparative Studies of the Ham Characteristic of Hot-dry Wind and High Temperature Heat Waves. *Adv. Earth Sci.* **2009**, *24*, 865–873.
41. Lu, A.; Ge, J.; Pang, D.; He, Y.; Pang, H. Asynchronous Response of Droughts to ENSO in China. *J. Glaciol. Geocryol.* **2006**, *28*, 535–542. [[CrossRef](#)]
42. Zheng, Y.; Dong, L.; Xia, Q.; Liang, C.; Wang, L.; Shao, Y. Effects of revegetation on climate in the Mu Us Sandy Land of China. *Sci. Total Environ.* **2020**, *739*, 139958. [[CrossRef](#)]
43. Lu, J. Evaluation of Vegetation Restoration in Loess Plateau and Time-Lag Effect of Climate Change and Drought. Master’s Dissertation, Northwest A&F University, Xianyang, China, 2022. [[CrossRef](#)]
44. Wei, X.; He, W.; Zhou, Y.; Ju, W.; Xiao, J.; Li, X.; Liu, Y.; Xu, S.; Bi, W.; Zhang, X. Global assessment of lagged and cumulative effects of drought on grassland gross primary production. *Ecol. Indic* **2022**, *136*, 108646. [[CrossRef](#)]
45. Gao, W.; Zheng, C.; Liu, X.; Lu, Y.; Chen, Y.; Wei, Y.; Ma, Y. NDVI-based vegetation dynamics and their responses to climate change and human activities from 1982 to 2020: A case study in the Mu Us Sandy Land, China. *Ecol. Indic* **2022**, *137*, 108745. [[CrossRef](#)]
46. Wang, J. Drought Monitoring Based on TVDI and Its Lag Research in Hebei Province. Master’s Dissertation, Hebei University of Engineering, Handan, China, 2022. [[CrossRef](#)]
47. Wang, H.; Guo, Y.; Bai, Y.; Wang, N.; Wei, X.; Zhou, M. Dynamic pattern of vegetation in Xinjiang and its time-lag effect on climate. *Trans. Chin. Soc. Agric. Eng.* **2023**, *39*, 137–145.
48. Zheng, Q.; Wu, J.; Jiang, P. Numerical study on the effect of the distribution of the southeast sealine of china on the amplifying of the torrential rain of the landing typhoon 9216. *J. Trop. Meteorol.* **1996**, *12*, 17–26.
49. Wang, S.; Li, R.; Wu, Y.; Zhao, S. Effects of multi-temporal scale drought on vegetation dynamics in Inner Mongolia from 1982 to 2015, China. *Ecol. Indic* **2022**, *136*, 108666. [[CrossRef](#)]
50. Zhang, L.; Cheng, L.; Sun, Y.; Pang, Y.; Li, J.; Jia, X.; Fei, B.; Xiu, X.; Yin, J.; Wu, B. Grain size characteristics of soil on typical underlying surfaces in Mu Us Sandy Land. *Chin. J. Ecol.* **2023**, 1–9. Available online: <https://link.cnki.net/urlid/21.1148.Q.20230906.1327.012> (accessed on 20 February 2024).

Disclaimer/Publisher’s Note: The statements, opinions and data contained in all publications are solely those of the individual author(s) and contributor(s) and not of MDPI and/or the editor(s). MDPI and/or the editor(s) disclaim responsibility for any injury to people or property resulting from any ideas, methods, instructions or products referred to in the content.